Kinetic Preference for Oriented DNA Binding by the Yeast TATA-Binding Protein TBP

Yichin Liu and Alanna Schepartz*

Department of Chemistry, Yale University, New Haven, Connecticut 06520-8107

Received August 21, 2000

ABSTRACT: In solution, the TATA box binding protein from *S. cerevisiae* (yTBP) is only minimally oriented when bound to the adenovirus major late promoter (AdMLP) and the yeast *CYC1* promoter. At equilibrium, approximately 60% of the complexes are assembled in the orientation observed within crystal structures; 40% are assembled in the opposite orientation. Here we use stopped-flow fluorescence resonance energy transfer (FRET) to study the association kinetics of the two TBP·TATA box orientational isomers. Kinetics were determined by monitoring FRET between a unique tryptophan residue engineered into either the C- or the N-terminal stirrup of the conserved C-terminal subunit of yeast TBP (yTBPc) and an aminocoumarin moiety appended either upstream or downstream of the TATA box. Together, these constructs permitted a simultaneous yet independent monitor of the kinetics of TBP binding in both orientations. Not only did our results provide an independent confirmation of the free energy difference between the two orientational isomers, but they also showed that the orientational binding preference at equilibrium is a result of a faster association rate when TBP binds DNA in the orientation observed in the crystal structure.

Gene expression in eukaryotes is regulated in large part by control of the rate of transcription initiation [for recent reviews, see (*1*−*3*)]. In the case of promoter-specific transcription by RNA polymerase II, transcription initiation requires the formation of a multiprotein preinitiation complex (PIC)[1] (*4*, *5*). In eukaryotes, the PIC consists of RNA polymerase II, Srb and Med factors, and general transcription factors including TFIIA, TFIIB, TFIID, TFIIE, TFIIF, and TFIIH [reviewed in (*6*, *7*)]. The general transcription factor TFIID is itself composed of the TATA-binding protein (TBP) and at least eight additional TBP-associated factors (TAFs) [reviewed in (*8*, *9*)]. Although TAFs enhance transcription of certain genes in response to transcriptional activators and coactivators [reviewed by (*10*−*12*)], the TBP subunit alone can bind the TATA box with high affinity and assemble a PIC capable of basal transcription levels. Moreover, in many cases, the rate of TBP binding to the TATA box controls the overall rate of transcription, both in the presence and in the absence of transcription activators (*13*−*17*).

The central role of TBP in PIC formation has stimulated considerable research on the structure of eukaryotic TBP, both alone and in complex with its DNA and protein partners. Early studies of the conserved C-terminal domain of yeast and plant TBP (TBPc) showed a structure containing two subdomains related by a pseudo-2-fold symmetry axis (Figure 1A) (*18*−*20*). Later studies on binary TBPc·TATA box complexes demonstrated that this symmetry extends to the interface with the TATA box. Greater than 80% of the TBP residues that contact the TATA box (consensus sequence of TATA$\frac{A}{T}$A$\frac{A}{T}$N) are conserved between the two subdomains (*18*−*20*). Despite the similarity between the two halves of the DNA-contact surface of TBPc, all eukaryotic TBPc·TATA crystal structures published to date show the protein bound to DNA in a single orientation (*18*−*20*). In this orientation, the C-terminal subdomain of TBPc interacts with the more conserved 5′ TATA half-site, and the N-terminal subdomain contacts the less conserved 3′$\frac{A}{T}$A$\frac{A}{T}$N half-site. Moreover, genetic evidence suggests that this orientation is preserved in vivo (*21*). Together, these genetic and structural observations have led to the prevailing view that TBP binds the TATA box in a single orientation, nucleates assembly of an orientationally defined PIC, and initiates transcription in one direction.

Recently, we reported affinity cleavage experiments demonstrating that, in solution, TBP from *S. cerevisiae* (yTBP) is only minimally oriented when bound to the adenovirus major late promoter (AdMLP) and the yeast *CYC1* promoter (*22*). These experiments showed that yTBP binds the asymmetric TATA boxes in these two promoters as mixtures of two orientational isomers that differ by a 180° rotation about the pseudo-dyad axis of the complex. Although the orientational isomer observed by crystallography is preferred, it is only marginally (0.3 kcal·mol^{-1}) more stable than the isomer in which yTBP is rotated 180°. This difference in binding energy corresponds to a 60:40 ratio of the two isomers at equilibrium. These results clearly indicated

* Correspondence should be addressed to this author. E-mail: alanna.schepartz@.yale.edu. Phone: (203) 432-5094. Fax: (203) 432-3486.

[1] Abbreviations: AdMLP, adenovirus major late promoter; AMCA-S, 7-amino-3-[[[(succinimidyl)oxy]carbonyl]methyl]-4-methylcoumarin-6-sulfonic acid; BSA, bovine serum albumin; βME, 2-mercaptoethanol; DNA, deoxyribonucleic acid; DTT, dithiothreitol; EDTA, ethylenediaminetetraacetic acid; EMSA, electrophoretic mobility shift assay; FRET, fluorescence resonance energy transfer; HPLC, high-performance liquid chromatography; IPTG, 1-thio-β-D-galactopyranoside; NP-40, Nonidet P-40; PIC, preinitiation complex; PMSF, phenylmethanesulfonyl fluoride; TBP, TATA-binding protein.

10.1021/bi0019794 CCC: $20.00 © 2001 American Chemical Society
Published on Web 05/04/2001

that, at equilibrium, TBP cannot specify a unique polarity when bound to these promoters in the absence of other transcription factors (*22*).

EXPERIMENTAL PROCEDURES

TBP Variants. The proteins used in our experiments contained seven consecutive N-terminal histidine residues fused through a six amino acid thrombin linker to residues 61−240 of yeast TBP (TBPc) or variants thereof. Plasmids encoding the K97W and E188W variants (Figure 1A) of TBPc (pYL-K97Wc and pYL-E188Wc, respectively) were prepared by site-directed mutagenesis (*23*) of p5J-yTBPc (*18*) obtained from Paul Sigler's laboratory at Yale University. Protein expression was performed as follows. Five-liter growths of BL21(DE3) cells were transformed with pYL-K97Wc or pYL-E188Wc in LB medium containing 200 μg/mL ampicillin and induced with 400 μM IPTG at 37 °C when the OD_{600} reached 0.8. Cells were grown for an additional 3 h at 37 °C, and the growth mixture was centrifuged at 8000 rpm at 4 °C for 8 min. The cell pellet that formed was resuspended in 50 mL of 1× Lysis Buffer (30 mM Tris, pH 7.5, 500 mM KCl, 400 mM ammonium acetate, 10 mM imidazole, 10% glycerol, 2 mM βME, 1 mM PMSF), chilled on ice, and sonicated (Branson Sonifier) (3 pulses of 45 s duration at 80% duty cycle). After centrifugation at 18 000 rpm and 4 °C to remove cell debris, the supernatant (approximately 50 mL) was incubated with 0.5 mL of Ni−NTA resin (Qiagen) (preequilibrated with 1× Lysis Buffer) for 2 h at 4 °C. The Ni−NTA resin was separated from the supernatant by centrifugation at 4 °C and 3000 rpm, and washed 3 times with 2 mL aliquots of 0.5× Lysis Buffer. The histidine-tagged TBPc variants were isolated by incubating the resin for 30 min at 4 °C in 2 mL of 0.5× Lysis Buffer containing 500 mM imidazole. The buffer was exchanged into Protein Buffer (30 mM Tris, pH 7.5, 50 mM KCl, 10% glycerol, 1 mM EDTA, 1 mM DTT) using a Centricon-10 (Amicon, Inc., Beverly, MA). TBP samples in approximately 10 mL of Protein Buffer were then loaded onto a 1 mL Hi-Trap Heparin column (Pharmacia Biotech) and eluted using a linear KCl gradient (50−800 mM). The TBP fractions that eluted at approximately 500 mM KCl were concentrated to micromolar concentration, and the amount of KCl was reduced to 50 mM using a Centricon-10. The purity of each TBPc sample was estimated to be greater than 99% by SDS−PAGE. Each protein sample was characterized by electrospray mass spectroscopy and amino acid analysis performed by the Yale Cancer Center Mass Spectrometry Resource and the HHMI Biopolymer Laboratory/W. M. Keck Foundation Biotechnology Resource Laboratory. In each case, the amino acid analyses and mass spectrometry data (E188W TBPc: found 21 842 Da, calculated 21 832 Da; K97W TBPc: found 21 834 Da, calculated 21 833 Da) agreed well with calculated values. Purified protein samples were stored at −70 °C.

DNA Synthesis and Labeling. AMCA-labeled oligonucleotides were synthesized and RP-HPLC purified by Synthetic Genetics (San Diego, CA). Oligonucleotides containing a single copy of the modified base Amino-Modifier C6 dT (Glen Research, Sterling, VA) were synthesized using standard phosphoramidite chemistry. Each modified oligonucleotide was then alkylated with 7-amino-3-[[[(succinimidyl)oxy]carbonyl]methyl]-4-methylcoumarin-6-sulfonic acid (AMCA-S, SE) (Molecular Probes, Eugene, OR) to produce AMCA-modified oligonucleotides containing the open T shown in Figure 1B. The purity of the purchased sample was assessed by RP-HPLC using an analytical RP Microsorb-MV 300 Å C18 column (Varian, Walnut Creek, CA) and an eluent containing 0.1 M triethylammonium acetate, pH 6.5, and between 2.5% and 65% acetonitrile. This analysis indicated that each AMCA-labeled oligonucleotide was greater than 99% pure. The identity of each AMCA-labeled oligonucleotide was confirmed by mass spectrometry. In each case, the calculated and found masses agreed well. The mass spectrometry data ($TATA_{22}^{up}$: found 6981 Da, calculated 6979 Da; $TATA_{22}^{down}$: found 7423 Da, calculated 7417 Da) agreed well with calculated values. Single-stranded modified oligonucleotides were annealed with the appropriate unlabeled complementary strands to generate the labeled duplexes $TATA_{22}^{up}$, $TATA_{22}^{down}$, and $TATA_{33}^{up}$ (Figure 1B). $TATA_{80}$ DNA used for footprinting and EMSA experiments comprised positions −64 to +16 of the AdMLP and was prepared as described (*22*).

Stopped-Flow Fluorescence. Experiments were performed at 25 °C by use of a KinTek SF-2001 stopped-flow spectrophotometer. All components used in FRET experiments were diluted in TBP Binding Buffer A (10 mM Tris, pH 7.4, 100 mM KCl, 2.5 mM $MgCl_2$, and 1 mM $CaCl_2$). To monitor the time-dependent change in FRET during the TBPc·TATA association reaction, a solution of 5 μM AMCA-labeled TATA DNA was diluted 10-fold into a 500 nM solution of TBP. Samples were irradiated at 285 nm, the wavelength where tryptophan excitation is maximal, with a Xenon short arc lamp (Ushio, Japan). Fluorescence emission was measured by photomultiplier tubes (PMT) mounted in two directions at 90° with respect to the exiting light. In one direction, the resulting emission passed through a 340 nm band-pass filter (12 nm bandwidth) (Corion, Holliston, MA) to detect tryptophan emission. In the opposite direction, a 435 nm long pass filter (Andover, Salem, NH) was used to detect AMCA emission.

$$[\mathrm{TBP}]_2 \underset{k_{on}^{dim}}{\overset{k_{off}^{dim}}{\rightleftharpoons}} 2\mathrm{TBP} \qquad \text{(A)}$$

$$\mathrm{TBP} + \mathrm{DNA} \underset{k_{off}^{2}}{\overset{k_{on}^{2}}{\rightleftharpoons}} [\mathrm{TBP{\cdot}DNA}]_{correct} \qquad \text{(B)}$$

$$\mathrm{TBP} + \mathrm{DNA} \underset{k_{off}^{3}}{\overset{k_{on}^{3}}{\rightleftharpoons}} [\mathrm{TBP{\cdot}DNA}]_{incorrect} \qquad \text{(C)}$$

The TBP and DNA samples were loaded into separate syringes, and the binding reaction was initiated by injecting both samples through a microjet mixer at a flow rate of 8 mL/s into the 20 μL observation cell. The injection flow rate and volume were controlled by a high-torque stepper motor drive with a dead time less than 1 ms. Between three and six traces recording the changes in AMCA and tryptophan emission intensity with time were averaged and compared to binding curves simulated by the KinTekSim program (*24*) using binding reactions A−C. Here, $[TBP{\cdot}DNA]_{correct}$ represents the concentration of the TBP·TATA isomer observed by crystallography, and $[TBP{\cdot}DNA]_{incorrect}$ represents the concentration of the orientational isomer in which TBP is rotated by 180° (Figure 1C). Two competitive processes were considered during our analysis: formation of the correct

complex and formation of the incorrect complex. Dissociation of the TBP dimer provides starting material for both of these processes. For any one TBP variant (K97W or E188W), two separate experiments were performed using different AMCA-labeled DNAs ($TATA_{22}^{up}$ or $TATA_{22}^{down}$) to assay the formation of the correct and incorrect complexes. The six rate constants describing the three equilibrium reactions (TBP dimerization, correct and incorrect complex formation) were obtained simultaneously from the single simulation that best described the changes in AMCA emission intensity.

Steady-State Fluorescence. Steady-state fluorescence spectra were acquired at 25 °C using either a SLM 4800s Fluorescence Spectrophotometer or a Photon Technology International (PTI) Quanta Master C60 Fluorescence Spectrophotometer. Components were diluted in TBP Binding Buffer A. The excitation wavelength was set at 280 nm for experiments with the SLM 4800s instrument or at 285 nm for experiments with the PTI C60 instrument. Each binding reaction contained a 1 μM sample of a TBPc variant in the presence or absence of 0.5 μM AMCA-labeled $TATA_{22}$ (for experiments with E188W TBP) or 1 μM AMCA-labeled $TATA_{22}$ (for experiments with K97W TBP). Unless indicated otherwise, binding reactions were preincubated for between 30 and 60 min to ensure that equilibrium had been reached. The fluorescence intensity was measured at 1 nm intervals between 300 and 470 nm.

Measurement of Fluorescence Resonance Energy Transfer Efficiency. The efficiency of FRET between a given donor and acceptor can be calculated from eq 1 (*25*):

$$E = \frac{R_o^6}{R_o^6 + R^6} \tag{1}$$

where E is the energy transfer efficiency, R is the distance between donor and acceptor (17 Å for the proximal pair and 35 Å for the distal pair), and R_o is the Forster radius at which energy transfer is 50% efficient. R_o for the tryptophan−AMCA pair used in our experiment was calculated according to eq 2:

$$R_o = 9786(\kappa^2 n^{-4} Q_D J)^{1/6} \text{ (units in Å)} \tag{2}$$

In this equation, κ^2 depends on the relative orientation of the donor and acceptor and is assumed to be 2/3 for a randomly oriented donor−acceptor pair (*26*); n represents the refractive index of the medium and has a value of 1.4 for proteins in water (*27*); Q_D represents the quantum yield of the donor which can be calculated according to eq 3 (*28*).

$$Q_D = Q_{RF}\left(\frac{I_D}{I_{RF}}\right)\left(\frac{A_{RF}}{A_D}\right) \tag{3}$$

In this equation, I_D and I_{RF} represent the experimentally determined fluorescence intensities (arbitrary units) of the tryptophan donor on E188W TBPc (I_D = 1 729 400) and the tryptophan reference (I_{RF} = 223 920), respectively; A represents the experimentally determined absorbance intensity (arbitrary units) of the tryptophan reference (A_{RF} = 600) or the actual donor in the protein (A_D = 4474); Q_{RF} represents the quantum yield of the tryptophan reference (Q_{RF} = 0.14) (*29*). The experimentally determined quantum yield (Q_D = 0.14) of the tryptophan in E188W TBPc was comparable to its reference compound, a free tryptophan residue. J in eq 2 represents the degree of overlap between donor emission and acceptor absorbance spectra as calculated according to eq 4 (*25*):

$$J = \frac{\sum F(\lambda)\epsilon(\lambda)\lambda^4 \Delta\lambda}{\sum F(\lambda)\Delta\lambda} \tag{4}$$

In this equation, $F(\lambda)$ represents the measured fluorescence intensity of the donor on the TBP proteins, and $\epsilon(\lambda)$ is the measured extinction coefficient of the acceptor on DNA at wavelength λ.

To estimate the efficiency of FRET between our tryptophan donor and AMCA acceptor, we acquired the absorbance spectrum of AMCA and the emission spectrum of tryptophan between 300 and 400 nm ($\Delta\lambda$ = 1 nm) in TBP Binding Buffer A at room temperature. Values of $F(\lambda)$ and $\epsilon(\lambda)$ were tabulated, and a value of $J = 1.75 \times 10^{-14}$ $M^{-1}cm^3$ was calculated using eq 4. The R_o and FRET efficiencies for the distal and proximal donor−acceptor pairs were calculated by substitution of this experimental value into eqs 2 and 1.

Footprinting of TBPc·TATA Complexes. MPE·Fe footprinting experiments were performed using a variation of the procedure described by Van Dyke and Dervan (*30, 31*). Briefly, binding reactions contained 150, 75, or 38 nM TBPc, E188W TBPc, or K97W TBPc and 1.3 nM 5′-[^{32}P]-$TATA_{80}$ in TBP Binding Buffer B [4 mM Tris, pH 8, 60 mM KCl, 5 mM $MgCl_2$, 4% glycerol, 0.1% NP-40, 0.04 mg/mL BSA, and 0.02 mg/mL poly(dG·dC)] and were incubated at 25 °C for 30 min. Separate cleavage reactions were performed using duplex oligonucleotides labeled on the top or the bottom strand. To each 5 μL binding reaction was added 1.5 μL of MPE·Fe-DTT cocktail [67 μM methidiumpropyl EDTA (Sigma), 0.052 mg/mL $Fe_2(NH_4)_2(SO_4)_2$, and 16.7 mM DTT], and the cleavage reactions were incubated for 10 min at 30 °C. The reactions were quenched by addition of 4 μL of formamide loading buffer (90% formamide in 1× TBE containing 0.1% each bromophenol blue and xylene cyanol FF) and frozen immediately on dry ice. The DNA in each reaction was denatured at 95 °C for 10 min and cooled on ice prior to denaturing electrophoresis [12% polyacrylamide (19:1 acrylamide:bis-acrylamide), 7 M urea in 1× TBE]. Gels were dried, and the radioactivity was quantified by use of a Storm 840 PhosphorImager (Molecular Dynamics).

Electrophoretic Mobility Shift Assay. TBPc (or variants thereof) at concentrations between 210 and 0.3 nM was incubated with 100 pM 5′-[^{32}P]-$TATA_{80}$ in TBP Binding Buffer B containing 0.06 mg/mL poly(dG·dC), 0.12 mg/mL BSA, and 0.5 mM DTT. Binding reactions were incubated at 25 °C for 30 min, and then applied to a 5% polyacrylamide gel (80:1 acrylamide:bis-acrylamide) prepared in 0.5× TBE containing 5 mM $MgCl_2$, 5% glycerol, and 0.5 mM DTT. Electrophoresis was performed in gel running buffer (0.5× TBE and 5 mM $MgCl_2$) at 250 V for 60 min at 25 °C, and the gels were analyzed using a Storm 840 PhosphoroImager. The equilibrium dissociation constant (K_d) of each TBP·TATA complex was determined using eq 5:

$$f = \frac{1}{1 + K_d/[\text{TBP}]} \tag{5}$$

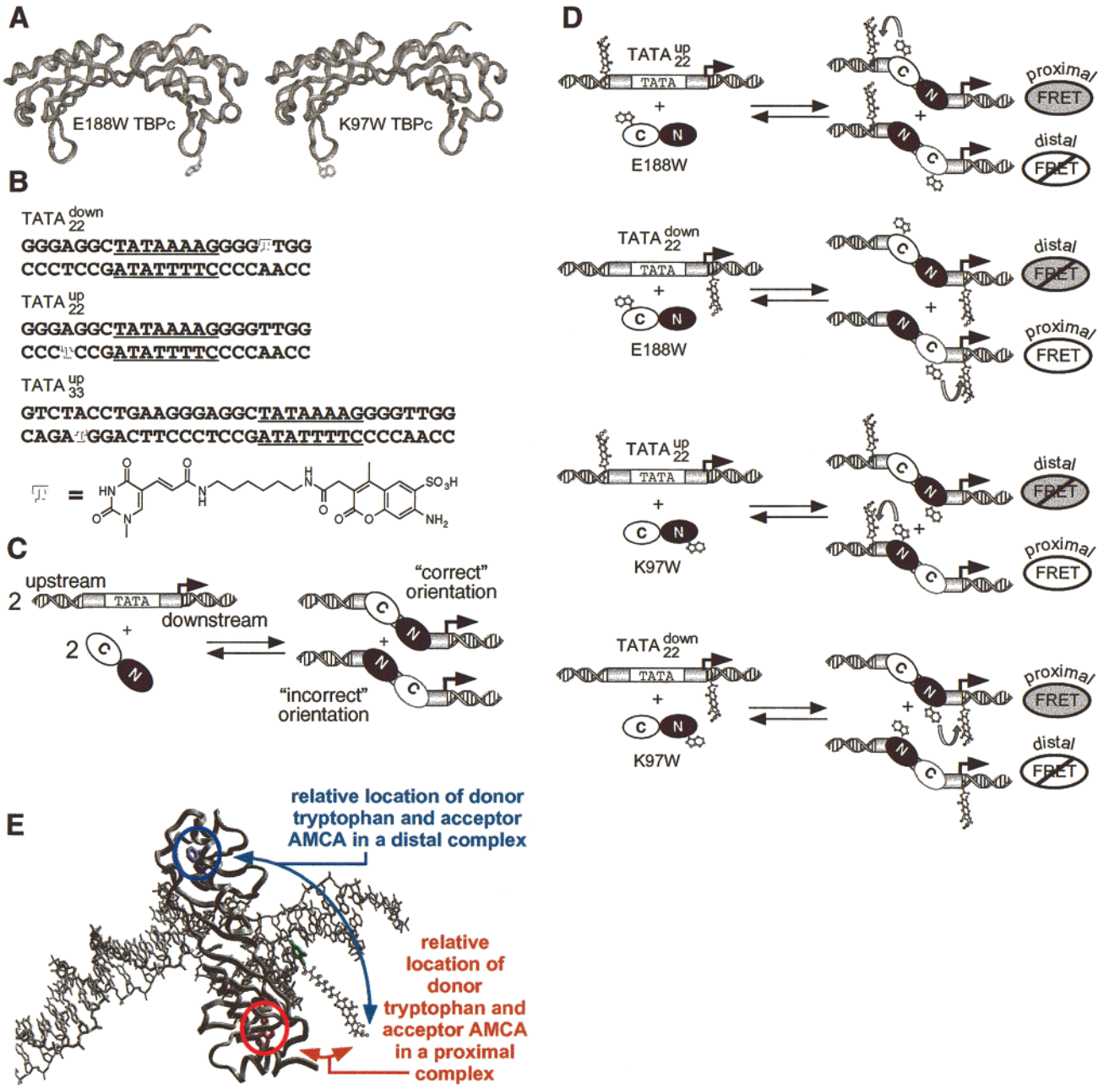

FIGURE 1: (A) Ribbon diagrams of the two TBPc variants used in this study, K97W TBPc and E188W TBPc. The locations of the unique tryptophan residues used as fluorescence resonance energy donors are shown explicitly. (B) Sequences of the duplex AMCA-modified oligonucleotides used for FRET experiments. Also shown is the location and structure of the AMCA-modified base T. (C) A cartoon illustrating formation of two orientational isomers in the binding reaction between TBPc and TATA DNA. The "correct" orientation represents the one seen in crystal structures of eukaryotic TBPc·TATA complexes (*18*−*20*); the "incorrect" orientation represents the one detected by affinity cleavage experiments (*22*) performed in solution. (D) A cartoon illustrating the two isomeric complexes formed in binding reactions containing either K97W TBPc or E188W TBPc and either $TATA_{22}^{up}$ or $TATA_{22}^{down}$. "Correct" complexes are indicated by gray-shaded ellipses; "incorrect" complexes by unshaded ellipses. Also indicated is the likelihood that each complex will exhibit FRET. AMCA and tryptophan moieties are shown explicitly and enlarged for clarity. (E) A top view of the TBPc·TATA complex with E188W and K97W mutations on the protein and modified T base covalently linked to AMCA upstream of the TATA box.

where *f* is the fraction of $TATA_{80}$ bound to TBP and [TBP] represents the total protein concentration.

RESULTS AND DISCUSSION

Experimental Design. To distinguish the association and dissociation kinetics of the two isomeric TBP·TATA complexes, we prepared two TBPc variants that each contained a unique tryptophan donor (Figure 1A) and two oligonucleotide duplexes that each contained a unique AMCA acceptor (Figure 1B). The tryptophan donor was located within either the N-terminal (for K97W) or the C-terminal (for E188W) stirrup loop of TBPc, the conserved C-terminal core yeast TBP. The AMCA acceptor was appended to a thymine residue located either 8 bp upstream ($TATA_{22}^{up}$) or 8 bp downstream ($TATA_{22}^{down}$) of the center of the TATA box (Figure 1A,B). Each TBP variant can bind each of the two DNAs in two orientations (Figure 1C). In one orientation, the appended AMCA acceptor is close to the unique

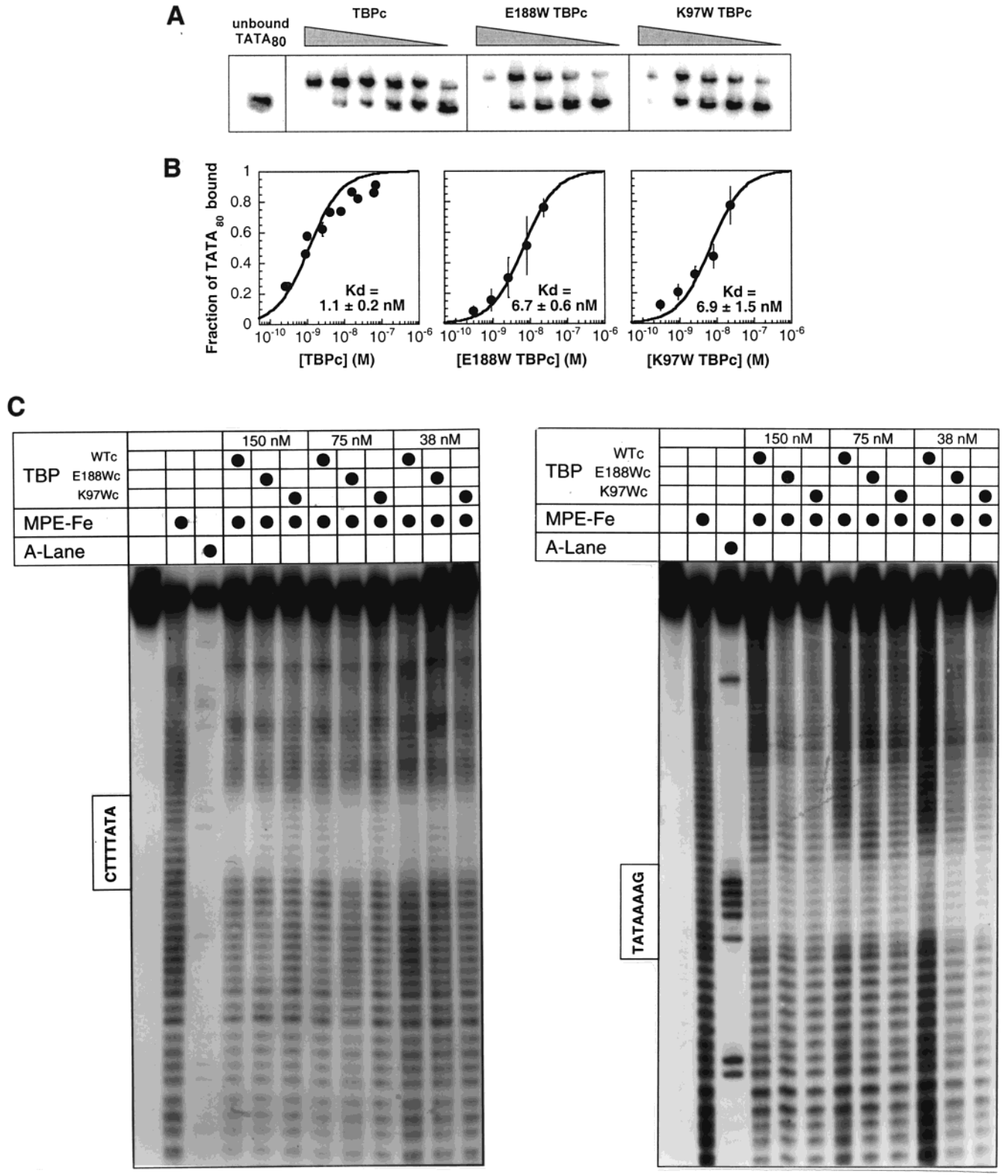

FIGURE 2: Equilibrium DNA binding by WT TBPc and K97W and E188W TBPc variants. (A) Autoradiogram of a native 5% gel illustrating binding of $TATA_{80}$ DNA by TBPc's in electrophoretic mobility shift assays. The relative concentration of each protein is depicted by the wedge; precise protein concentrations ranged between 70 and 0.3 nM. (B) Binding isotherms generated from EMSA data. Each point represents the average of at least three independent experiments. Error bars represent the standard error. The curve shown represents the best fit of the data to the Langmuir equation describing formation of 1:1 protein·DNA complex (*50, 51*). (C) Autoradiogram of a 12% denaturing gel illustrating the sequence dependence of DNA cleavage by MPE-Fe (*30, 31*) in the presence or absence of TBPc or variants thereof.

tryptophan residue in TBP (the proximal complex), whereas in the opposite orientation the appended AMCA is far from the unique tryptophan (the distal complex) (Figure 1D). As described below, we expect significant FRET only within proximal complexes. As a result, comparison of the kinetics describing association of any one TBP variant with

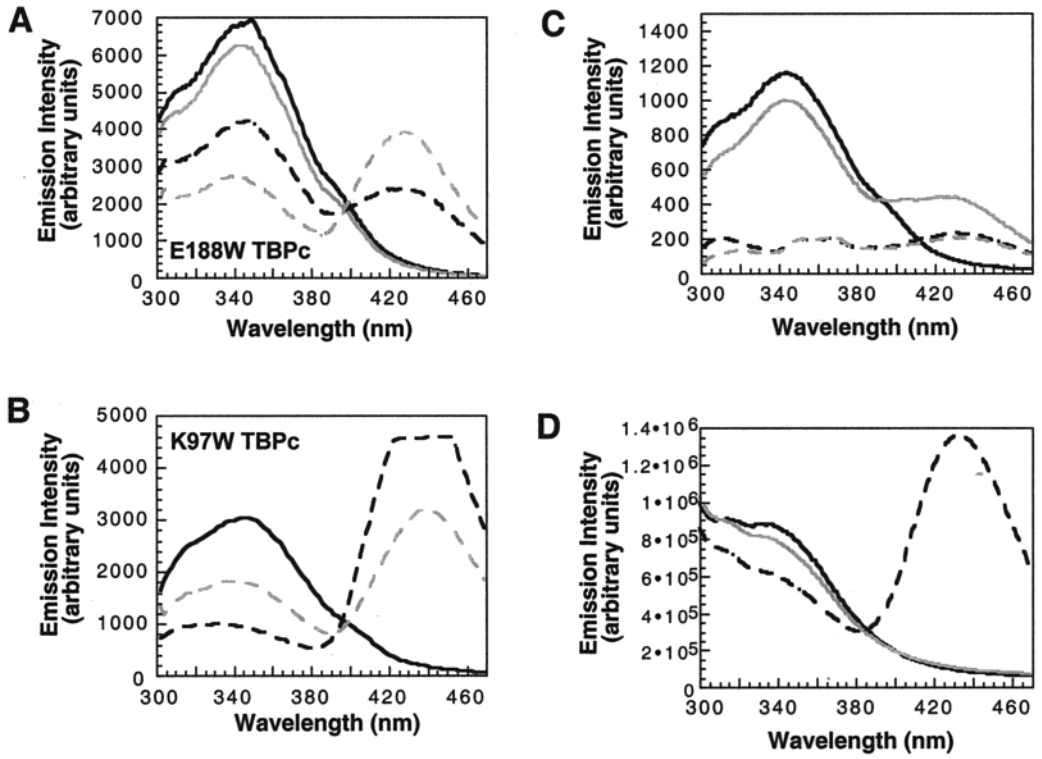

FIGURE 3: Steady-state FRET spectra of K97W and E188W TBPc's. (A) Emission spectra of 1 μM E188W TBPc alone (black solid), with 0.5 μM unlabeled $TATA_{22}$ (gray solid), with 0.5 μM $TATA_{22}^{down}$ (black dash, illustrating FRET from within the "correct" complex), and with $TATA_{22}^{up}$ (gray dash, illustrating FRET from within the "incorrect" complex). (B) Emission spectra of 1 μM K97W TBPc alone (black solid), with 1 μM $TATA_{22}^{down}$ (black dash, illustrating FRET from within the "incorrect" complex), and with 1 μM $TATA_{22}^{up}$ (gray dash, illustrating FRET from within the "correct" complex). (C) Emission spectra of 500 nM E188W TBPc alone (black solid) or with 100 nM $TATA_{22}^{down}$ (gray solid), and of 100 nM $TATA_{22}^{down}$ alone (gray dash) or with 425 nM TBPc (black dash). (D) Emission spectra of 300 nM E188W TBPc with 500 nM $TATA_{22}$ (black solid), 500 nM $TATA_{33}^{up}$ (gray), or 500 nM $TATA_{22}^{up}$ (black dash).

$TATA_{22}^{up}$ and $TATA_{22}^{down}$ provides a relative measure of the association rate constants for forming the two TBP·TATA orientational isomers. Using both TBP variants provides an additional, independent control for the accuracy of our results.

Choice of the Donor−Acceptor Pair. Our choice of AMCA as the FRET acceptor and its location relative to the TATA box were designed to maximize the difference in FRET efficiency between proximal and distal donor−acceptor pairs. The absorption spectrum of AMCA almost completely overlaps the emission spectrum of tryptophan (data not shown), yet its extinction coefficient at $\lambda_{max} = 353$ nm is small [$\epsilon(353\text{ nm}) = 19\,000\ M^{-1}\ cm^{-1}$] compared to other fluorescent probes (*32*). These factors combine to give rise to a relatively short $R_o = 27$ Å for this donor−acceptor pair. Using the crystal structure of yTBPc·TATA as a guide (*18*, *19*), we estimate that the β-carbon of residue 97 or 188 in TBPc within a proximal complex is located less than 17 Å from the methyl group on C5 of the T base (Figure 1D,E). By contrast, the analogous distance within a distal complex was estimated to be greater than 35 Å (Figure 1D,E), well above R_o. These distances predict a FRET efficiency of greater than 94% for transfer within a proximal complex and less than 17% for transfer within a distal complex. We anticipate that FRET efficiency within a distal complex will be limited further by a reduced orientation factor κ^2 that arises because the tethered AMCA moiety is placed within the DNA major groove, pointing away from the tryptophan on the TBPc stirrup loop (Figure 1E). Thus, because it is characterized by a reduced orientation factor κ^2 (*33*), FRET efficiency within the distal complex is expected to be significantly less than 17%.

Preparation and Characterization of TBPc Variants. K97W and E188W TBPc were prepared and characterized as described under Experimental Procedures. We used electrophoretic mobility shift analysis (*34*, *35*) and MPE·Fe footprinting (*30*, *31*) to evaluate the affinity and specificity of DNA binding by each protein (Figure 2). K97W and E188W TBPc bound TATA-containing $TATA_{80}$ DNA to form complexes with equilibrium dissociation constants below 7 nM, similar to the 1 nM K_d displayed by WT TBPc·$TATA_{80}$ under identical conditions. In addition, we observed no difference in the concentration dependence, size, or locations of hypersensitive sites within MPE·Fe footprints produced by K97W, E188W, and WT TBPc (Figure 2C). Finally, none of the proteins displayed high nonspecific DNA binding or protein aggregation even at concentrations as high as 150 nM. These results confirmed that the DNA-binding properties of K97W and E188W TBPc's effectively mimicked that of WT TBPc.

Initial Steady-State FRET Experiments and Controls. First we performed steady-state FRET experiments to determine the ratio of orientational isomers of K97W TBPc·TATA or of E188W TBPc·TATA at equilibrium. Our goal was to verify that introduction of the donor tryptophan at position 97 or 188 did not alter the distribution of orientational isomers. Spectra were recorded at 25 °C and at a concentration of 1 μM protein and 1 μM DNA for experiments with

K97W TBPc and with 0.5 μM DNA for experiments with E188W TBPc (Figure 3). The spectrum of E188W TBPc alone was characterized by an emission maximum at 340 nm, precisely the value expected for tryptophan, and no emission at 435 nm (Figure 3A). Addition of unlabeled $TATA_{22}$ DNA caused little change in the wavelength or intensity of emission. Addition of $TATA_{22}^{up}$, however, resulted in a 60% decrease in the intensity of tryptophan emission at 340 nm and a concomitant increase in AMCA emission at 435 nm. A smaller decrease in emission at 340 nm and increase in 435 nm were observed when E188W TBPc was mixed with $TATA_{22}^{down}$ (Figure 3A). Our experimental design predicts (Figure 1D) that the relative decrease in emission at 340 nm upon addition of $TATA_{22}^{up}$ and $TATA_{22}^{down}$ to E188W TBPc estimates the equilibrium ratio of the correct and incorrect orientational isomers, respectively. This analysis yielded a ratio of 3:2, in excellent agreement with the ratio expected on the basis of affinity cleavage (*22*). A similar ratio was calculated from an analogous experiment performed with K97W TBPc (Figure 3B). No FRET was observed when $TATA_{22}^{down}$ was mixed with WT TBPc (Figure 3C), confirming that the FRET observed with E188W and K97W TBP was due to transfer to AMCA from the tryptophan in the TBP stirrup and not from other residues within the protein.

A control experiment was performed to confirm the prediction that FRET efficiency within distal complexes would be negligible. This experiment made use of $TATA_{33}^{up}$, an oligonucleotide duplex in which the AMCA acceptor was appended to the same helical face as in $TATA_{22}^{up}$, but one helical turn further upstream from the TATA box. This shift placed the AMCA acceptor approximately 49 Å from the donor tryptophan in a proximal complex and was predicted to decrease FRET efficiency from 94% to 3%. As expected, the emission spectrum of E188W TBPc in the presence of $TATA_{33}^{up}$ showed no evidence of FRET (Figure 3D). This experiment provides additional support that the increases in emission observed at 435 nm result from FRET within a proximal complex.

As a final prelude to our kinetics studies, we assessed the time period required for DNA binding by TBPc or variants thereof. A 500 nM sample of E188W TBPc was mixed with 100, 200, 500, and 800 nM $TATA_{22}^{down}$, and the emission spectra were measured after 5 and 60 min (Figure 4A,B). The extent of FRET, as reflected by either the decrease in emission at 340 nm or the increase at 420 nm, was proportional to the concentration of $TATA_{22}^{down}$ (Figure 4A,B) and identical at the two time points tested.

The Rates of TBP·TATA Complex Formation Were Measured by Stopped-Flow Fluorescence. The time-dependent increase in FRET upon formation of each fluorescent TBPc·DNA complex was monitored at 340 nm (tryptophan emission) and at 435 nm (AMCA emission) after diluting 1 volume of 5 μM AMCA-labeled DNA into 10 volumes of 500 nM K97W or E188W TBPc (Figure 5A,B). Approximately 90% of the total change in AMCA emission occurred in a fast phase within 1 s of mixing (Figure 5C,D). During the fast phase, there was an excellent correlation between the rate of tryptophan donor quenching and AMCA acceptor excitation for both TBP variants (Figure 5C,D). This fast phase was followed by a slow phase that occurred over

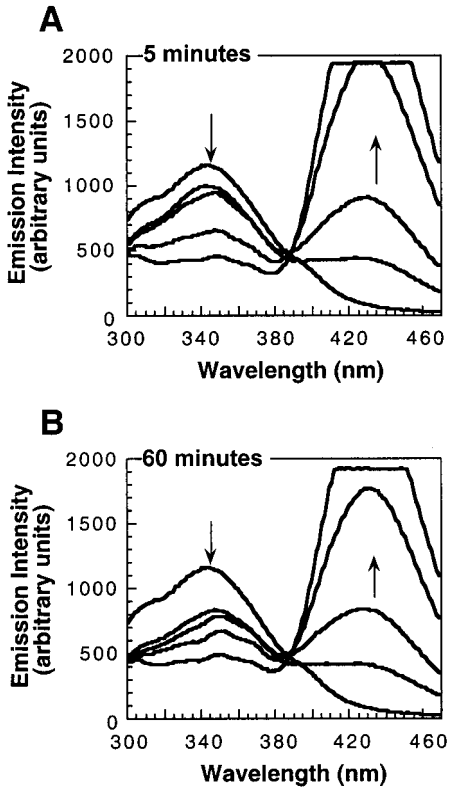

FIGURE 4: Concentration dependence of FRET between E188W TBPc and $TATA_{22}^{down}$ after 5 and 60 min incubation. (A) FRET measured after a 5 min incubation between 500 nM E188W and no DNA, 100 nM $TATA_{22}^{down}$, 200 nM $TATA_{22}^{down}$, 500 nM $TATA_{22}^{down}$, or 800 nM $TATA_{22}^{down}$ (order follows the direction of arrows). (B) FRET measured after a 60 min binding incubation of the same reactants as in (A).

10 s and accounted for the remaining intensity change (Figure 5A,B). The slow phase observed in the AMCA spectra corresponded to a monophasic increase in emission intensity; the slow phase observed in the tryptophan spectra corresponded to an initial increase and then a decrease in emission intensity. Rate constants were derived from AMCA emission spectra only, as the time-dependent increase in AMCA emission results only from FRET within a TBP·TATA complex. By contrast, the time-dependent change in tryptophan emission intensity results also from changes in the TBP monomer−dimer equilibrium.

TBP·TATA Orientational Isomers Associate at Different Rates. The time-dependent changes in AMCA emission intensity produced upon DNA binding by K97W and E188W TBPc variants were simulated using models that lacked or included a TBP monomer−dimer equilibrium (eqs A−C). The rates of formation of both TBP·TATA orientational isomers were simulated concurrently using the KinTek program (*24*). Rate constants were adjusted such that the simulation accurately reproduced the experimental curves. For both proteins, inclusion of the TBP monomer−dimer equilibrium (eq A) dramatically improved the quality of the fit (compare black and gray residual plots in Figure 6A and Figure 6B). The best fit to the data yielded an equilibrium dissociation constant K_{dim} of 2.8 ± 0.8 μM for the E188W TBPc dimer; this equilibrium constant was defined by an association rate constant k_{on}^{dim} of (3 ± 2) × 10^5 M^{-1} s^{-1} and dissociation rate constant k_{off}^{dim} of 0.85 ± 0.02 s^{-1} (Figure 6A). Similarly, the best fit to the data acquired with K97W

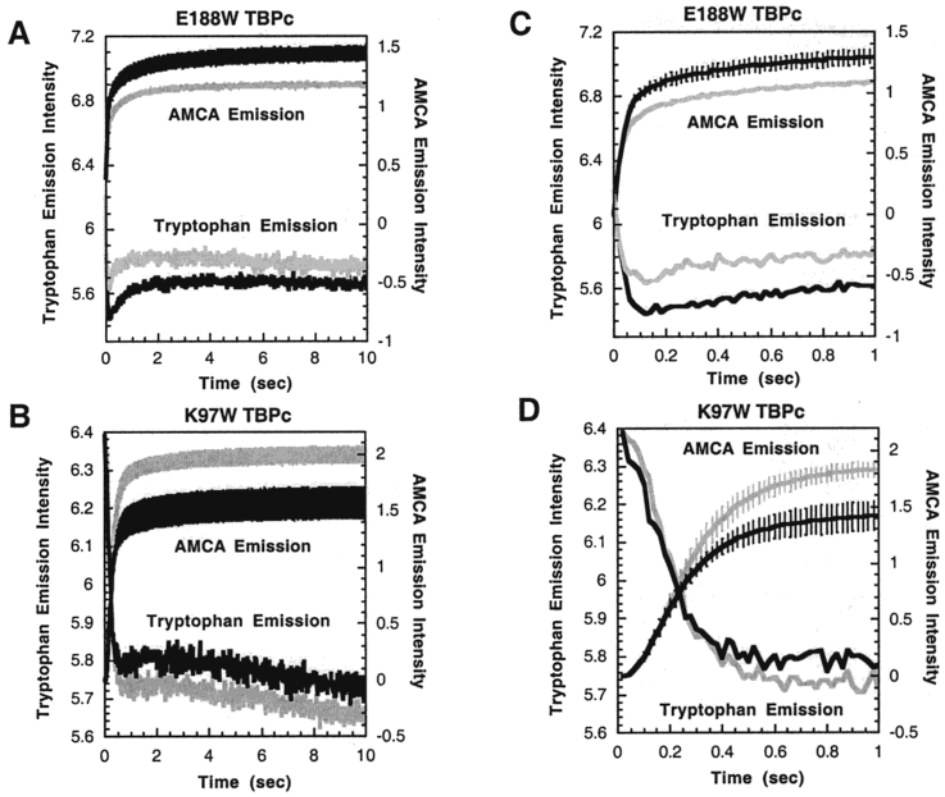

FIGURE 5: Plots illustrating the correlation between the time-dependent changes in AMCA and tryptophan emission following rapid-mixing of E188W TBPc (A) or K97W TBPc (B) with $TATA_{22}^{up}$ (black) or $TATA_{22}^{down}$ (gray). Plots showing the first 1 s of binding reaction for E188W TBPc (C) or K97W TBPc (D) [same color scheme as (A) and (B)].

yielded a equilibrium dissociation constant of 4.5 ± 0.2 μM for the K97W TBPc dimer; this equilibrium constant was defined by a similar association rate constant k_{on}^{dim} of (2 ± 1) × 10^5 M^{-1} s^{-1} and dissociation rate constant k_{off}^{dim} of 0.90 ± 0.05 s^{-1}.

The TBPc dimer equilibrium dissociation constant we deduce here (2.8−4.5 μM) is higher than that measured by biochemical pull-down assays (4 nM) performed in a Tris−acetate buffer containing glycerol, BSA, NP-40, spermidine, and poly(dG·dC) (*36*−*38*). However, our value agrees well with that obtained from sedimentation and analytical ultracentrifugation studies performed with yeast TBP in a buffer close to our own (*39*−*42*). Moreover, independent measurement of the time-dependent change in tryptophan fluorescence upon 60-fold dilution of 25 μM E188W TBPc suggested a K_{dim} value 6.5 ± 0.1 μM under our experimental conditions (data not shown). An equilibrium dissociation constant in the micromolar concentration range predicts a small but significant (between 11 and 27%) population of TBPc dimers at $t = 0$ during our kinetics experiment. Thus, we assigned the fast phase seen in the AMCA spectra to a burst of DNA binding by TBPc monomers present at the start of the reaction, and the slow phase to DNA binding by monomers generated by dissociation of TBPc dimers.

We used the same E188W TBPc dimerization rate constants [k_{on}^{dim} = (3 ± 2) × 10^5 M^{-1} $s^{-1}$and k_{off}^{dim} = 0.85 ± 0.02 s^{-1}] to simulate the AMCA emission curves resulting from formation of the correct and incorrect E188W·TATA orientational isomers (Figure 6A). The best fit resulted from association rate constants k_{on}^2 = (3.00 ± 0.02) × 10^7 M^{-1} s^{-1} (formation of the correct isomer) and k_{on}^3 = (2.10 ± 0.02) × 10^7 M^{-1} s^{-1} (formation of the incorrect orientational isomer); both complexes required the same $k_{off}^2 = k_{off}^3$ = 0.04 ± 0.001 s^{-1}. These rate constants define an equilibrium dissociation constant of 1.3 nM for the correct E188W TBPc·TATA complex and 1.9 nM for the incorrect E188W TBPc·TATA complex, in the range expected on the basis of electrophoretic mobility shift assays (Figure 2). The ratio of the two complexes at equilibrium is 59:41, in excellent agreement with the 60:40 ratio observed in previous DNA affinity cleavage experiments (*22*). It is notable that the fit to the experimental data suffered significantly when the values for k_{on}^2 and k_{on}^3 were constrained to identical values (Figure 6C).

A similar analysis was performed with the K97W TBPc variant. In this case, we used K97W TBPc dimerization rate constants [k_{on}^{dim} = (2 ± 1) × 10^5 M^{-1} s^{-1} and k_{off}^{dim} = 0.90 ± 0.05 s^{-1}] to simulate the two AMCA emission spectra (Figure 6B). In this case, the best fit resulted from association rate constants k_{on}^2 = (1.30 ± 0.01) × 10^7 M^{-1} s^{-1} (for formation of the correct isomer) and k_{on}^3 = (0.90 ± 0.01) × 10^7 M^{-1} s^{-1} (formation of the incorrect isomer); both complexes required the same dissociation rate constant $k_{off}^2 = k_{off}^3$ = 0.150 ± 0.002 s^{-1}. These rate constants define equilibrium dissociation constants of 12 and 17 nM for the correct and incorrect K97W·TATA isomers, respectively. As expected, the ratio of the two complexes at equilibrium is 59:41, in excellent agreement with the ratio of E188W·TATA isomers obtained experimentally in this work and the 60:40 ratio observed in the previous DNA affinity cleavage experiments (*22*). Again, the fit to the experimental data suffered

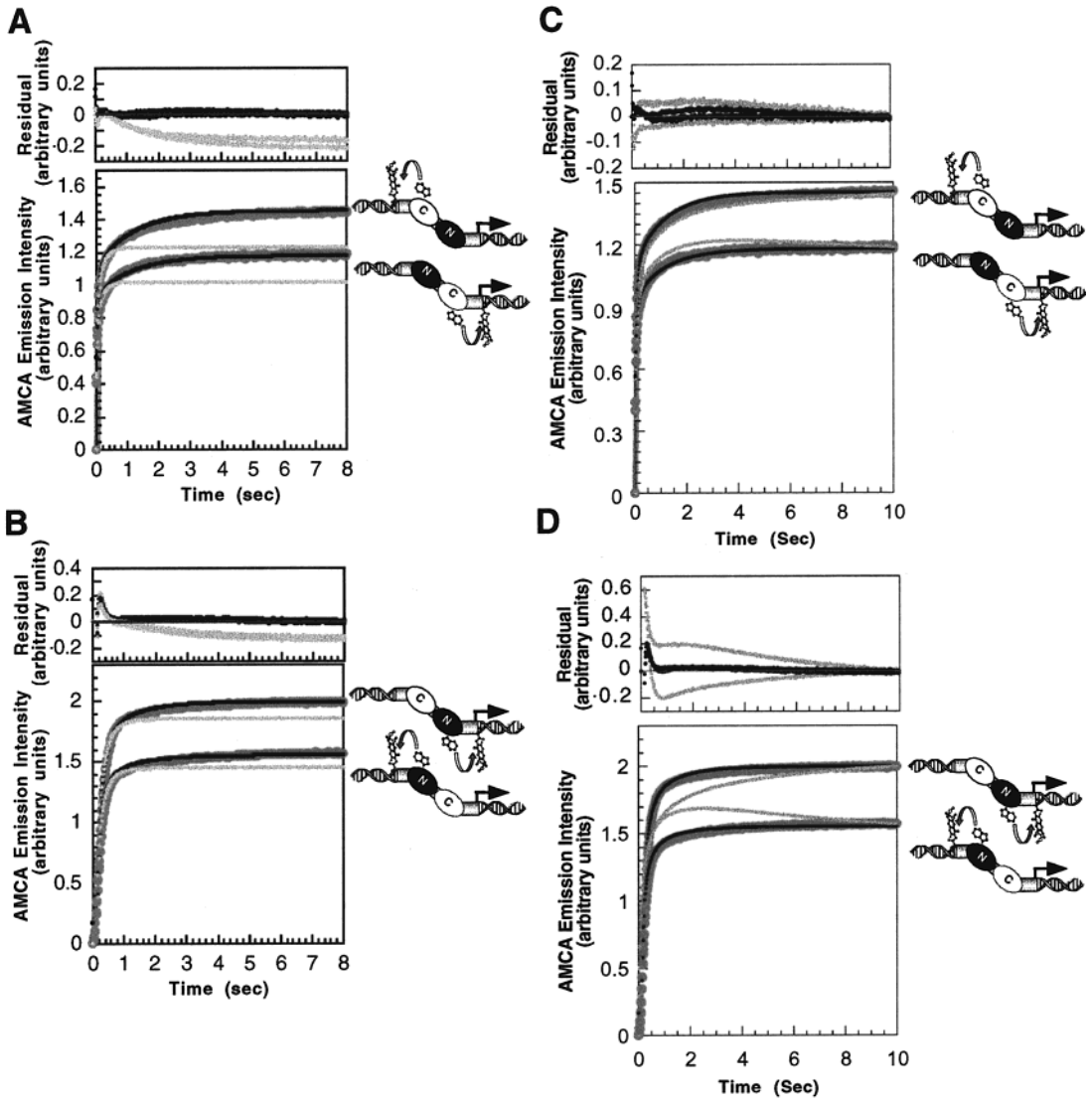

FIGURE 6: Time dependence of FRET between variant TBPc's and AMCA-labeled DNA. (A) Plot illustrating the change in AMCA emission following rapid-mixing of E188W TBPc with $TATA_{22}^{up}$ (complex A shown in Figure 1D) or $TATA_{22}^{down}$ (complex B shown in Figure 1D). The lines represent the best fit of the experimental data to the TBP·DNA binding reaction (Figure 5C) in the presence (black) or in the absence (gray) of TBP dimer. Residual values were the deviation of the fits in the presence (black) or in the absence (gray) of TBP dimer from experimental values. (B) Same plot illustrating AMCA emission change was performed for K97W TBPc (complex C and D shown in Figure 1D). Kinetic traces acquired over 0.5 and 100 s were consistent with the 10 s scan (data not shown). (C and D) Plots illustrating a poor fit (gray) to the experimental data when the values for k_{on}^2 and k_{on}^3 were constrained to an identical value. Black lines illustrate the same fit shown in panels A and B.

significantly when the values for k_{on}^2 and k_{on}^3 were constrained to identical values (Figure 6D).

The rate constants we measure for association of TBPc·TATA complexes are 10−100-fold larger than those reported previously (*43, 44*). For example, the value we report is 10-fold larger than that reported by Parkhurst, and 100-fold higher than that reported by Perez-Howard, for association of complexes containing full-length TBP (*43, 44*). This difference could be caused by differences in TBP length, the presence of tryptophan at position 97 or 188, and the absence of glycerol in our buffer, as well as by the kinetic modeling of our data. N-terminal truncated TBPc forms a more stable TBP·TATA complex (*45*), and it is reasonable that a fraction of the increased stability at equilibrium is reflected by a larger association rate constant. In addition, glycerol can significantly slow the association of protein·DNA complexes by increasing the viscosity of the medium (*46, 47*). Despite the discrepancies in the absolute values of the rate constants determined under different in vitro conditions, differences in the molecular environment that TBP encounters when binding TATA DNA in one orientation versus the other are likely to be relatively independent of solution conditions. Thus, the mechanistic basis for the orientational preference defined by our kinetics studies is likely to be valid in vitro and, more importantly, in vivo.

A Kinetic Preference for Orientated TATA Box Binding by TBP. Taken together, our results suggest that the 3:2 equilibrium preference of TBPc for the orientational isomer seen by crystallography is due to a difference in association rate constant. In the case of both E188W and K97W TBPc, the ratio of the two association rate constants k_{on}^2:k_{on}^3 is 59:41, in excellent agreement with the ratio of equilibrium isomers determined by DNA affinity cleavage experiments (*22*). By contrast, the rate constants describing dissociation of the isomeric complexes k_{off}^2 and k_{off}^3 were identical: For

E188W, the values were 0.040 ± 0.001 s^{-1}; for K97W, the value was 0.150 ± 0.002 s^{-1}. Although the difference in the association rate constants is relatively small (~20%), the difference accurately reflects the difference in the equilibrium constants deduced from equilibrium affinity cleavage experiments. Any larger difference in the association rate constant would be inconsistent with the difference in equilibrium constants reported earlier.

A Kinetic Preference for Oriented TBP·TATA Complex Formation: Implications for Preinitiation Complex Assembly. What structural features might lead to more rapid assembly of the TBPc·TATA isomer observed by crystallography? Several structural differences between the C- and N-terminal TATA-recognition surfaces of TBPc and between the two halves of the TATA box sequence exist, and were invoked initially to explain observation of a single orientational isomer in early TBP·TATA crystal structures. These differences include sequence and electrostatic differences between the N- and C-terminal subdomains of TBPc and the demonstrated flexibility difference between the two halves of the TATA box (*18*, *19*, *48*, *49*). For example, it has been proposed that the larger side chains (*48*) and a proline (*49*) on the interior β-sheet of the C-terminal subdomain would interact more favorably with the more flexible 5′ half of the TATA box (*48*). It has also been proposed that binding and bending of the more rigid 3′ half of the TATA box by the more electropositive N-terminal TBPc subdomain is enthalpically favorable compared to binding by the C-terminal subdomain (*18*). Both proposals could account for the lower activation barrier for forming the preferred TBPc·TATA isomeric complex. To the extent that this kinetic preference is preserved in vivo, the higher population of properly oriented TBP·TATA complexes could be trapped by accretion of other members of the preinitiation complex, whether they assemble in a stepwise fashion or in a single, holoenzyme-directed step.

ACKNOWLEDGMENT

We are grateful to the late Professor Paul Sigler (Yale University) for generous gifts of wild-type yTBPc protein and expression clone.

REFERENCES

1. Goodbourn, S. (1996) Oxford, New York.
2. Kuras, L., and Struhl, K. (1999) *Nature 399*, 609−612.
3. Li, X.-Y., Virbasius, A., Zhu, X., and Green, M. R. (1999) *Nature 399*, 605−609.
4. Hernandez, N. (1993) *Genes Dev. 7*, 1291−1308.
5. White, R. J., and Jackson, S. P. (1992) *Cell 71*, 1041−1053.
6. Roeder, R. G. (1996) *Trends Biochem. Sci. 21*, 327−334.
7. Tjian, R. (1996) *Philos. Trans. R. Soc. London B 351*, 491−499.
8. Burley, S. K., and Roeder, R. G. (1996) *Annu. Rev. Biochem. 65*, 769−799.
9. Lee, T. I., and Young, R. A. (1998) *Genes Dev. 12*, 1398−1408.
10. Tjian, R., and Maniatis, T. (1994) *Cell 77*, 5−8.
11. Verrijzer, C. P., Yokomori, K., Chen, J. L., and Tjian, R. (1994) *Science 264*, 933−941.
12. Ranish, J. A., and Hahn, S. (1996) *Curr. Opin. Genet. Dev. 6*, 151−158.
13. Klein, C., and Struhl, K. (1994) *Science 266*, 280−282.
14. Chatterjee, S., and Struhl, K. (1995) *Nature 374*, 820−822.
15. Colgan, J., and Manley, J. L. (1992) *Genes Dev. 6*, 304−315.
16. Klages, N., and Strubin, M. (1995) *Nature 374*, 822−823.
17. Lieberman, P. M., and Berk, A. J. (1994) *Genes Dev. 8*, 995−1006.
18. Kim, Y., Geiger, J. H., Hahn, S., and Sigler, P. B. (1993) *Nature 365*, 512−520.
19. Kim, J. L., Nikolov, D. B., and Burley, S. K. (1993) *Nature 365*, 520−527.
20. Miaskiewicz, K., and Ornstein, R. L. (1996) *J. Biomol. Struct. Dyn. 13*, 593−600.
21. Klug, A. (1993) *Gene 135*, 83−92.
22. Cox, J. M., Hayward, M. M., Sanchez, J. F., Gegnas, L. D., van der Zee, S., et al. (1997) *Proc. Natl. Acad. Sci. U.S.A. 94*, 13475−13480.
23. Kunkel, T. A., Roberts, J. D., and Zakour, R. A. (1987) *Methods Enzymol. 154*, 367−377.
24. Barshop, B. A., Wrenn, R. F., and Frieden, C. (1983) *Anal. Biochem. 130*, 134−145.
25. Förster, T. (1948) *Ann. Phys. 2*, 55−75.
26. Chapman, E. R., Alexander, K., Vorherr, T., Carafoli, E., and Storm, D. R. (1992) *Biochemistry 31*, 12819−12825.
27. Lackowicz, J. R. (1983) *Principles of Fluorescence Spectroscopy*, Plenum Press, New York.
28. Epps, D. E., Poorman, R., Hui, J., Carlson, W., and Heinrikson, J. (1987) *J. Biol. Chem. 262*, 10570−10573.
29. Chabbert, M., Lukas, T. J., Watterson, D. M., Axelson, P. H., and Prendergast, F. G. (1991) *Biochemistry 30*, 7615−7630.
30. Van Dyke, M. W., and Dervan, P. B. (1983) *Nucleic Acids Res. 11*, 5555−5567.
31. Van Dyke, M. W., and Dervan, P. B. (1983) *Biochemistry 22*, 2373−2377.
32. Wu, P., and Brand, L. (1994) *Anal. Biochem. 218*, 1−13.
33. Fairclough, R. H., and Cantor, C. R. (1978) *Methods Enzymol. 48*, 347−379.
34. Fried, M., and Crothers, D. M. (1981) *Nucleic Acids Res. 9*, 6505−6525.
35. Garner, M. M., and Revzin, A. (1981) *Nucleic Acids Res. 9*, 3047−3060.
36. Coleman, R. A., Taggart, A. K., Benjamin, L. R., and Pugh, B. F. (1995) *J. Biol. Chem. 270*, 13842−13849.
37. Coleman, R. A., and Pugh, B. F. (1997) *Proc. Natl. Acad. Sci. U.S.A. 94*, 7221−7226.
38. Coleman, R. A., Taggart, A. K. P., Burma, S., J. J. C., II, and Pugh, B. F. (1999) *Mol. Cells 4*, 451−457.
39. Petri, V., Hsieh, M., Jamison, E., and Brenowitz, M. (1998) *Biochemistry 37*, 15842−15849.
40. Daugherty, M., Brenowitz, M., and Fried, M. G. (1999) *J. Mol. Biol. 285*, 1389−1399.
41. Parkhurst, K. M., Richards, R. M., Brenowitz, M., and Parkhurst, L. J. (1999) *J. Mol. Biol. 289*, 1327−1341.
42. Campbell, K. M., Ranallo, R. T., Stargell, L. A., and Lumb, K. J. (2000) *Biochemistry 39*, 2633−2638.
43. Parkhurst, K. M., Brenowitz, M., and Parkhurst, L. J. (1996) *Biochemistry 35*, 7459−7465.
44. Perez-Howard, G. M., Weil, P. A., and Beechem, J. M. (1995)-*Biochemistry 34*, 8005−8017.
45. Horikoshi, M., Yamamoto, T., Ohkuma, Y., and Weil, A. P. (1990) *Cell 61*, 1171−1178.
46. Feltzer, R. E., Gray, R. D., Dean, W. L., and Pierce, X. (2000)-*J. Biol. Chem. 275*, 21002−21009.
47. Gutfreund, H. (1995) *Kinetics for the life sciences*, Cambridge University Press, Cambridge, U.K.
48. Suzuki, M., Allen, M. D., Yagi, N., and Finch, J. T. (1996) *Nucleic Acids Res. 24*, 2767−2773.
49. Juo, Z. S., Chiu, T. K., Leiberman, P. M., Baikalov, I., Berk, A. J., et al. (1996) *J. Mol. Biol. 261*, 239−254.
50. Metallo, S. J., and Schepartz, A. (1994) *Chem. Biol. 1*, 143−151.
51. Cuenoud, B., and Schepartz, A. (1993) *Science 259*, 510−513.

BI0019794